BULLETIN OF THE POLISH ACADEMY OF SCIENCES
TECHNICAL SCIENCES, Vol. 60, No. 4, 2012
DOI: 10.2478/v10175-012-0098-2

Ultrasonic-vibration assisted arc-welding of aluminum alloys

A. KRAJEWSKI[1]*, W. WŁOSIŃSKI[2], T. CHMIELEWSKI[1], and P. KOŁODZIEJCZAK[1]

[1] Department of Joining Engineering, Institute of Materials Processing Faculty of Production Engineering, Warsaw University of Technology, 85 Narbutta St., 02-524 Warsaw, Poland
[2] Polish Academy of Sciences, 1 Defilad Sq., 00-901 Warsaw, Poland

Abstract. The structure and hardness of the surface-welds and fusion-welds made on a 2017A aluminum alloy waveguide using the MIG and TIG methods with and without the participation of ultrasonic vibrations were examined. Cross-sections of the fusions and surface-welds thus obtained were observed in a microscope and the hardness distributions were determined.

The aim of the study was to analyze the effects of the ultrasonic vibrations applied to the melted metal pool by a vibrating substrate which in our experiments was a waveguide. The interactions of the ultrasonic vibrations with the molten metal during its solidification and also with the heat-affected zone were examined at various phases of the vibration wave. The ultrasonic vibrations affected the structure of a weld. These changes are strongly depended on the wave phase.

Key words: ultrasonic vibrations, MIG/TIG welding, aluminum alloys, structure, microhardness.

1. Introduction

Studies performed thus far have shown that mechanical vibrations affect in an obvious manner the structure and properties of welded joints [1–3]. Irrespective of the parent metal and the welding method, the vibrations change the structure in both the melted zone and the heat-affected zone (HAZ). The literature reports describe various ways of introducing vibrations into the welding zone, such as e.g. electric-arc vibrations [4, 5], thermal effects of a coherent laser beam [6], or the direct introduction of the vibrations into the material through a waveguide [7].

Most authors are not, however, concerned with the technical aspects of the mechanical vibration-enhance welding operation, whereas in order to control the phenomena that then occur and to describe quantitatively their influence on the final structures in a reliable manner, these aspects seem to be crucial. It is also important to examine the effect of the phase and amplitude of the vibration wave on the structure and properties of the welds. In view of the increasing use of aluminum alloys in the automobile and aircraft industries with the aim to reduce the weight of the vehicles while preserving the rigidity and mechanical strength of their structure, the need has arisen for high-quality welding joints. The possibility of welding the aluminum alloys with a high quality of the welded structures is the key problem in the manufacture of automobiles, aircraft and sporting equipment. The methods of improving the weldability without the need for heat treatments are especially interesting since they give chance to reduce the production costs and time-consumption. The problems of improving the weldability of aluminum alloys and steel are discussed in [7]. The authors achieved a reduction of the grain size and hardness of the welds, and their decrease in the heat-affected zone. However, the methods of introducing the vibrations into the welding zone, the control of their amplitude and energy seem to be unclear and doubtful.

The authors of ref. [8] used the GTA method for welding the high-strength 7075 aluminum alloy subjecting it to mechanical vibrations with the frequency ranging from 105 Hz to 2050 Hz. At frequencies of 1025 Hz and 2050 Hz, they observed a decrease of the susceptibility to hot-cracking of the weld, but it increased again at 2051 Hz. Welding at frequencies from 1025 Hz to 2050 Hz gave a refining of the structure, more effective than welding at lower frequencies. The joint welded without the assistance of vibrations had a coarse-grained structure.

The application of mechanical vibrations in welding processes leading to the improvement of the structure and properties of the welded joints is also described in refs [9–14].

In general, it can be concluded that the mechanical vibrations improve the structure and mechanical properties of certain zones of welded joints. Other investigators [15] used ultrasonic vibration-enhanced laser welding which improved the regularity of the weld-face shape, increased the depth of the fusion, and reduced the probability of the occurrence of cracks and porosity thanks to the decrease of the turbulent flow in the molten pool.

In order to achieve the desired structural changes and advantageous properties of the fusions and surface-welds welded with the assistance of vibrations, it is necessary to control fully the course of the vibration wave, the direction of its introduction, and also to have under control the heat cycle. Publications which analyze the effect of the vibration parameters on the structure and properties of welded structures are scarce [11–15], which may be associated with the great difficulties, encountered in the mechanical vibration-assisted

*e-mail: akrajew@wip.pw.edu.pl

welding processes with controlling the effect of heat on the vibrating system.

Our earlier experiments [1–3] have shown that whether the changes occurring in a given zone of the weld due to vibrations are positive or negative they depend on the vibration wave phase. The present paper describes the results of the analysis of the effect of the ultrasound wave phase on the individual zones which are formed during arc-welding.

Moreover, there are potential chances of employing the mechanical vibrations in conventional welding processes. In certain applications it may be important to produce homogenous composite protective coatings based on ceramic or intermetallic materials [16–18], to develop methods involving the periodic variation of pressure in the melting pool as e.g. is the case in plasma-hardfacing [19] or in the segregation and agglomeration of the structural components [20, 21], or even to intensification of solid state diffusion [22, 23], and finally in all welding processes where the mechanical properties of the weld can be modified by modifying the material structure [24]. In all these processes, mechanical vibrations may have advantageous effect and improve the mechanical properties of the final product, provided that the process of their propagation is fully controlled.

2. Strain-stress relationship

To select the characteristic and representative regions for structural and hardness examinations we analyzed the strain-stress behavior of the ultrasonic vibrations and the elastic stresses induced in the elastic medium i.e. in a 2017A alloy waveguide with the length z equal to the wavelength λ. The vibration parameters adopted in the analysis were: frequency $f = 20$ kHz, amplitude $A = 10$ μm, wavelength $\lambda = 0.254$ m equal to the waveguide length, the 2017A aluminum alloy density $\rho = 2800$ kg/m^3, wave velocity in solid state of aluminum alloy $c = 5080$ m/s, Poisson ratio $\nu = 0.33$, and Young modulus $E = 72.5$ GPa.

It has been assumed that the longitudinal displacement ε_L and transverse displacement ε_T for standing wave are given by (1, 2) [25, 26]:

$$\varepsilon_L = A\left[\cos\left(2\pi f\frac{\lambda}{c}+\varphi\right)+\cos\left(2\pi f\frac{\lambda}{c}-\varphi\right)\right], \quad (1)$$

$$\varepsilon_T = -A\nu\left[\cos\left(2\pi f\frac{\lambda}{c}+\varphi\right)+\cos\left(2\pi f\frac{\lambda}{c}-\varphi\right)\right], \quad (2)$$

where φ is the phase shift angle (0-2π).

The pressure of the vibration, longitudinal stress σ, the transverse (shear) stress τ, and the stresses reduced according to the Huber hypothesis σ_Z were calculated respectively from (3–6):

$$P = 2\pi\rho f c A, \quad (3)$$

$$\sigma = P\left[\cos\left(2\pi f\frac{\lambda}{c}+\varphi\right)+\cos\left(2\pi f\frac{\lambda}{c}-\varphi\right)\right], \quad (4)$$

$$\tau = -\nu P\left[\cos\left(2\pi f\frac{\lambda}{c}+\varphi\right)+\cos\left(2\pi f\frac{\lambda}{c}-\varphi\right)\right], \quad (5)$$

$$\sigma_Z = \sqrt{\frac{\sigma^2}{2}+3\tau^2}. \quad (6)$$

Figures 1 and 2 show the displacements (deformations) and stresses induced in the waveguide by the vibrations.

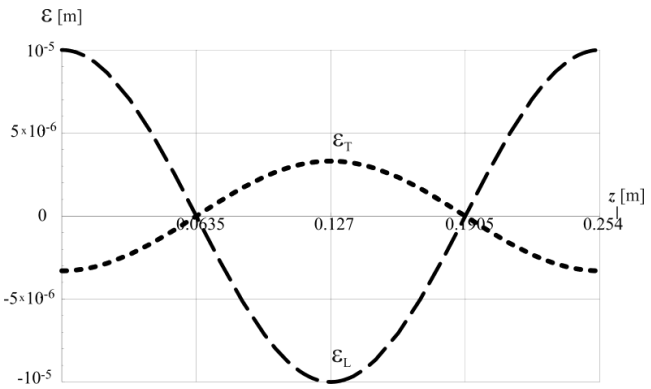

Fig. 1. Longitudinal displacement ε_L and transversal displacement ε_T in a waveguide with the length $z = \lambda$

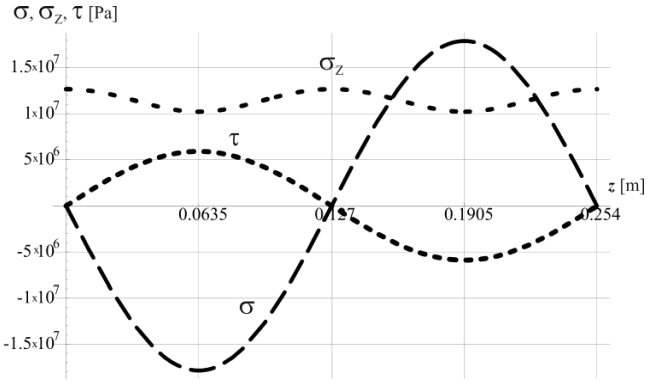

Fig. 2. Distribution of axial stresses σ, transverse stresses τ, and reduced stresses σ_Z in a waveguide with the length $z = \lambda$

The spatial variation of the displacements and stresses versus z induced in an elastic medium with the waveguide length is shown in Fig. 3.

It can be seen from Figs. 1–3 that there is symmetry in the vibration wave between the regions: 1/4λ, 3/4λ, and $\lambda = 0$, 1/2λ, λ. This symmetry accrued because of stagnant character of vibration wave in waveguide. Hence, to find the representative results for the characteristic regions of the waveguide, it is sufficient to examine the structures and hardness only in two selected regions, such as e.g. at the distance $z = 1/2\lambda = 0.127$ m and $z = 3/4\lambda = 0.1905$ m from the fixture point of the waveguide in the vibrating system.

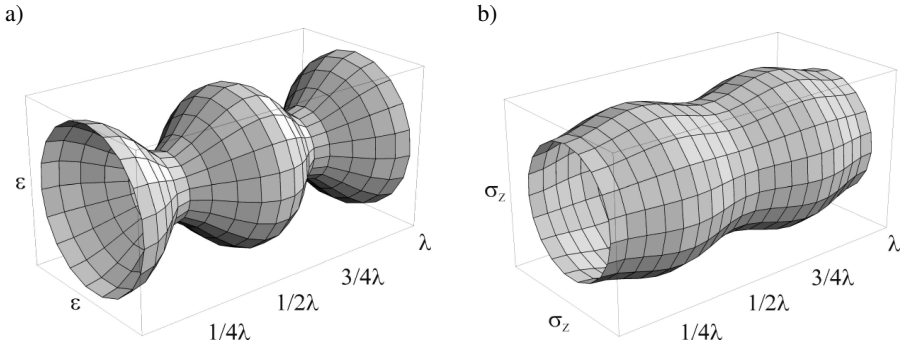

Fig. 3. Spatial distribution of: a) displacements, b) the stresses reduced according to the Huber hypothesis along the length of a waveguide with $z = \lambda$

3. Experiments

The experiments included surface-welding and fusing on a 2017A aluminum alloy waveguide in the form of a cylinder 0.045m in diameter and 0.254 m long using the MIG and TIG methods. The waveguide length was selected so that it was equal to the wavelength 1 λ (corresponding to a vibration frequency of 20 kHz). The study had the comparative character i.e. the structure and hardness of the various welds obtained with and without the participation of ultrasonic vibrations were compared. Even though the 2017A alloy is commonly considered to be difficult to weld because of the increased probability of stress-induced corrosion, its mechanical properties are very interesting in spite of its low density. The chemical composition and some properties of the used materials are given in Table 1.

The experimental set-up (Fig. 4) consisted of a waveguide coupled, through a concentrator, with a ceramic transducer supplied from a GUZ 20 2500 W ultrasonic generator, manufactured by the Tele-Radiotechnical Institute, an ARISTOTIG 200 AC/DC welding machine designed for TIG welding (ESAB Co.), a Fronius ALU Edition source intended for the MIG method, and a mechanized set for straight-line welding (Fronius Co), which was coupled with the welding equipment so that the start of the arc and the start of the head travel were synchronized. In both techniques examined the welding holder was fixed to an arm of the mechanized set and positioned to be suitable for flat welding (the main axis of the torch positioned vertically).

Table 1
Chemical composition and properties of the materials used in the experiments [27, 28]

2017	Si	Fe	Cu	Mn	Mg	Cr	Zn	Ti
	0.5	0.7	4	0.7	0.6	0.1	0.25	0.15
	T_L[°C]	T_S[°C]	R_m [MPa]	R_e [MPa]	E [GPa]	ν	ρ [kg/m^3]	k [W/mK]
	510	645	380	250	72.5	0.33	$2.8 \cdot 10^3$	170
5056	Si	Fe	Cu	Mn	Mg	Cr	Zn	Ti
	0.08	0.7	0.01	0.11	4.9	0.07	0.03	0.06
	T_L [°C]	T_S [°C]	R_m [MPa]	R_e [MPa]	E [GPa]	ν	ρ [kg/m^3]	k [W/mK]
	500	630	250	220	65	0.30	$2.8 \cdot 10^3$	125

T_L, T_S – liquidus and solidus temperature, R_e – plasticity limit, R_m, – ultimate tensile strength, E – Young module, k – coefficient of thermal conductivity, ν – Poisson ratio, ρ – density

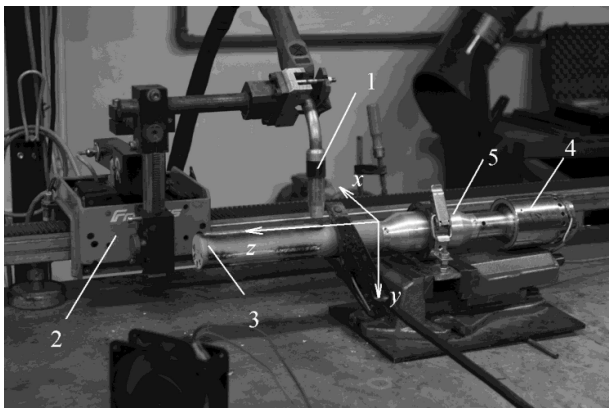

Fig. 4. Experimental set-up: 1 – welding torch, 2 – linear manipulator, 3 – waveguide, 4 – ultrasonic transducer, 5 – concentrator

In TIG welding, the electrode was made of WC 20 Grey tungsten with a diameter of 2.4 mm and a spherical tip. The molten pool was protected by argon, flown at a rate of 11 l/min. The supply was an alternating or constant electric current of intensity of 150 A and frequency of 30 Hz. The welding speed was 0.0025 m/s.

In MIG welding we used a 5056 aluminum alloy wire 1.2 mm in diameter. The process was also entirely automated. Also in this experiment the gas protecting the molten pool was argon with a flow rate of 17 l/min. The electric current intensity was 167 A, the arc voltage was 19.4 V, and the welding speed was 0.0122 m/s.

After each pass of the welding head, the waveguide was cooled to a room temperature. The consecutive fusions were welded along the cylinder generator, at every 45°, so as to prevent the subsequent thermal cycles from affecting each other.

Figure 5 shows the appearance of the fusion-welds obtained by TIG AC, with and without the participation of ultrasounds. We can see great differences between the welds produced with and without the assistance of ultrasound. The weld produced without the participation of ultrasonic vibrations (Fig. 5a, b) contains local open porosity, its weld-face is uniform, flat, and free of unevenness which is observed after ultrasonic welding. It can also be seen that the fusion line is 'jerked', discontinuous, and, in the central region of the weld face, a distinguishable lighter-color zone, 1.5 mm wide, occurs.

In the photographs showing the two zones characteristic of the course of the ultrasonic wave (Fig. 5b, c) we can see significant differences in the appearance of the weld face. At $z = 0.127$ m, (1/2λ), which is the distance from the fixed waveguide end, there appear characteristic surface irregularities of the weld face, pores, and mechanically-induced discontinuity. At the distance $z = 0.1905$ m (3/4λ) these weld-face irregularities and pores disappear, whereas the weld-face/parent material interfaces are much more regular and free of the characteristic unevenness observed after welding without the assistance of ultrasonic vibrations. The wall of the waveguide touching the weld face shows characteristic scorches which are evidence that the argon protection was unstable.

The best uniformity of the weld-face is obtained when the node of the ultrasonic vibration wave is at $z = 0.1905$ m (3/4λ) – Fig. 5c. In order to prevent the frequencies of the alternating electric current and of the mechanical vibration from superposing, we decided to use a DC supply, even though it is not usually used in welding aluminum alloys. Fig. 6 shows photographs of the welds obtained by the TIG DC method. The oxidized surface of the weld produced without the participation of vibrations (Fig. 6a) was cracked, which is natural in DC welding (no cathodal scattering effect). Such cracks were not observed in welding with the assistance of ultrasonic vibrations applied in the compressive stress activity region at $z = 0.1905$ m (3/4λ). This has never been obtained earlier in DC welding.

After the ultrasound-assisted welding, the weld-face showed considerable unevenness at the distance $z = 0.127$ m (1/2λ) from the fixed waveguide end (Fig. 6b), whereas at the distance $z = 0.1905$ m (3/4λ) the weld-face had a longitudinal concavity which could occur due to the compressive stresses induced at the node of the ultrasonic wave in this zone (Fig. 6c).

The appearance of a surface-weld obtained by MIG welding is shown in Fig. 7 (the face of the welds was about 8 mm wide and about 4 mm deep). We can see that the weld face appearance evidently depends on the phase of the standing wave established in the waveguide.

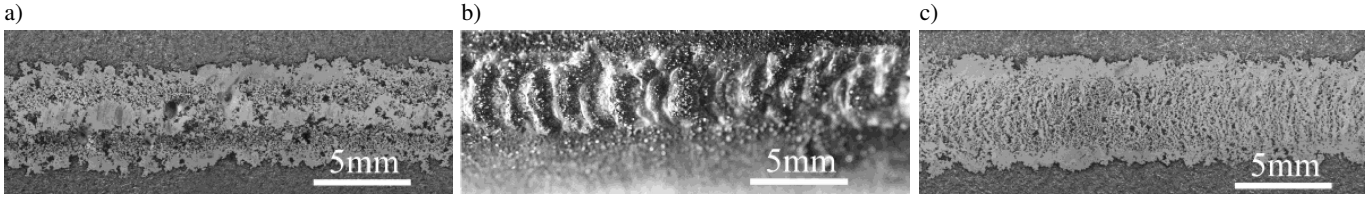

Fig. 5. TIG AC produced weld: (a) without vibrations (b) assisted with ultrasonic vibrations in the 0.127 m (1/2λ) region, and (c) with vibrations in the 0.1905 m region (3/4λ)

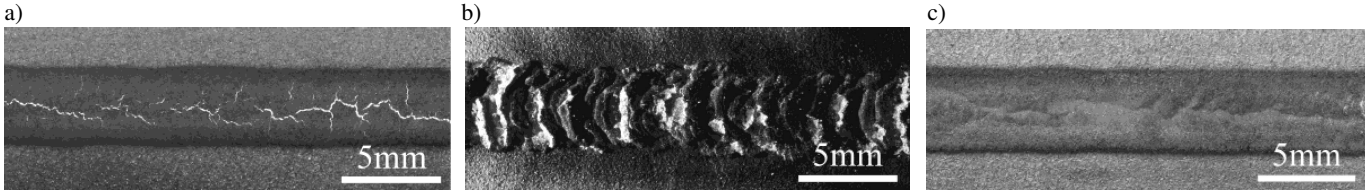

Fig. 6. TIG DC produced weld: (a) without vibrations within the (b) assisted with ultrasonic vibrations in the 0.127 m (1/2λ) region, and (c) with vibrations in the 0.1905m region (3/4λ)

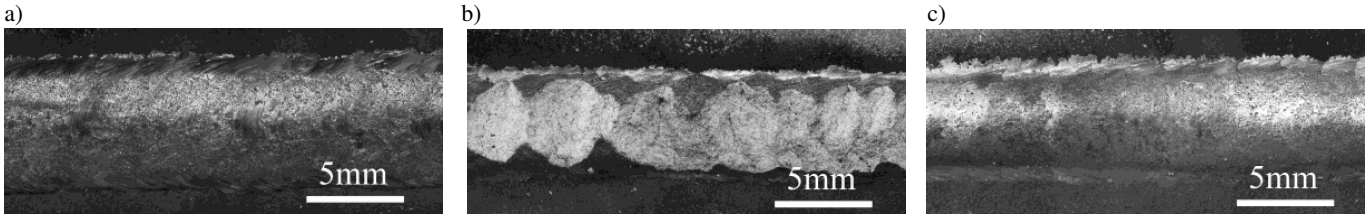

Fig. 7. MIG produced weld: (a) without vibrations (b) assisted with ultrasonic vibrations in the 0.127 m (1/2λ) region, and (c) with vibrations in the 0.1905 m region (3/4λ)

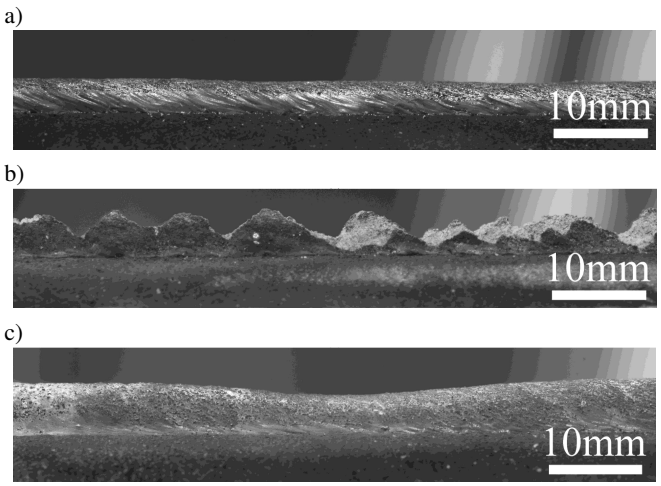

Fig. 8. Profile of the weld obtained by the MIG method (a) without the vibrations, (b) with ultrasonic vibrations within the region $z = 0.127$ m (1/2λ), and (c) with ultrasonic vibrations in the region $z = 0.1905$ m (3/4λ)

Figure 8 shows the profiles of the MIG welds with visible caves at $z = 0.1905$ m (Fig. 8c) and a "saw-toothed" vibration-induced discontinuity of the weld-face (Fig. 8b) which probably occurred as a result of the action of mechanical vibrations. The weld obtained by the MIG method has the face with a considerable height which varies with the coordinate z. At the distance $z = 0.1905$ m from the fixed waveguide end the weld face is caved into a depth of about 1 mm (Fig. 8c), whereas at $z = 0.127$ m it becomes discontinuous probably as a result of the ultrasonic vibration-induced deformation reaching a maximum (Fig. 8b).

The face of the weld obtained without the participation of ultrasounds has a constant height of about 2.5 mm. Pores are visible along its entire length, and they are much more numerous than those observed after the vibration-assisted welding.

The MIG and TIG welds were subjected to metallographic measurements. The cross-sections of these welds selected and appropriately prepared for these measurements ($z = 0.127$ and $z = 0.1905$ m), Figs. 9–17, were observed in a microscope and subjected to microhardness measurements.

Figures 12 and 13 are photographs of the structure of the TIG AC and TIG DC fusion welds, respectively. We can see that the TIG AC fusion produced without the ultrasound assistance (Fig. 12a) contains a considerable number of gaseous pores. The face of the ultrasound-assisted TIG DC weld (Fig. 12b) is characteristically caved at a distance of 190.5nm from the waveguide front end, but the weld grains do not show the directionality observed when the welding process is conducted without the participation of ultrasonic vibrations. In the TIG DC fusion (Fig. 13b) the introduction of ultrasounds results in well-marked changes in the bead structure occurring at a distance of 0.127 m from the waveguide front end. In both TIG AC/DC and MIG welds, the welding faces are cracked and porous, with the welding face spallings and discontinuities (Figs. 8b, 11b, 12b and 13b).

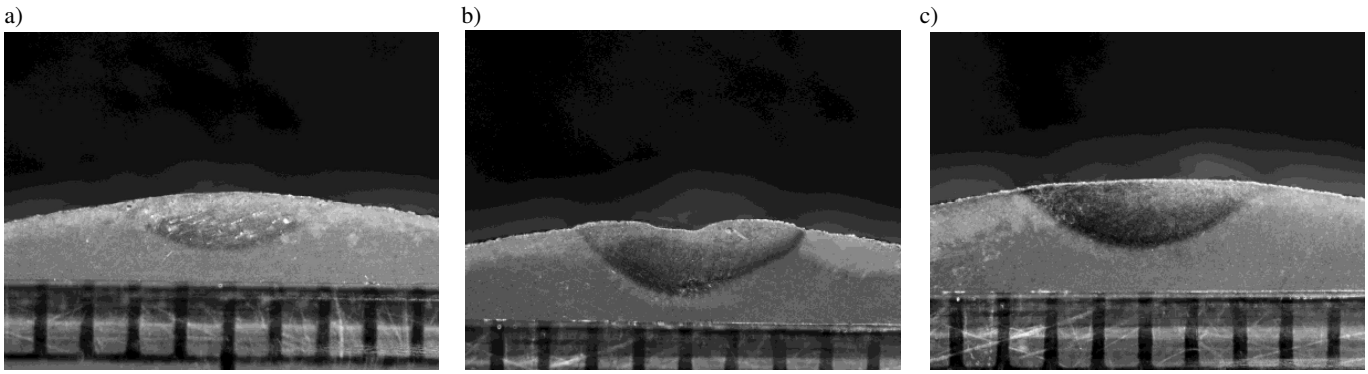

Fig. 9. Cross-section of the TIG AC welds: (a) without ultrasounds, (b) with the participation of ultrasounds at $z = 0.127$ m (1/2λ), and (c) with the participation of ultrasounds at z=0.1905m (3/4λ), visible scale-1 mm/div

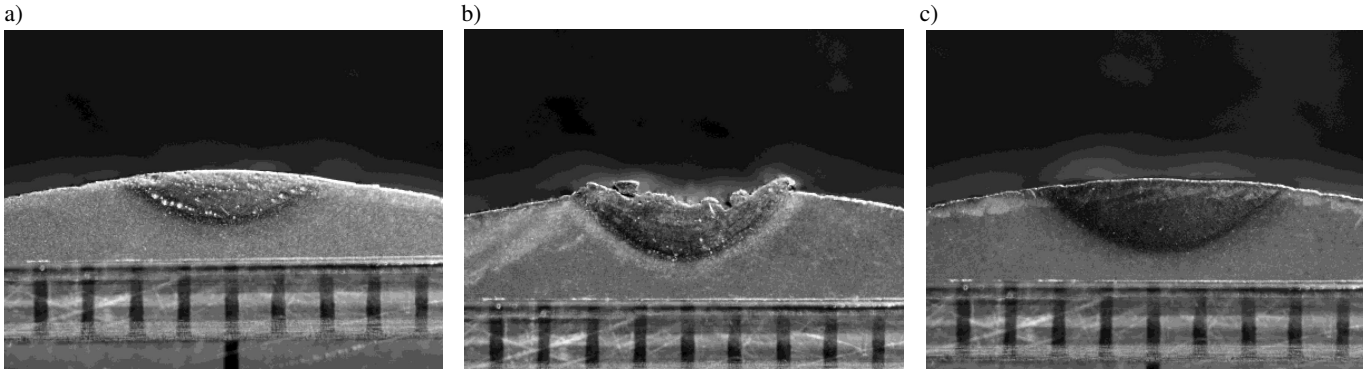

Fig. 10. Cross-section of the TIG DC welds: (a) without ultrasounds, (b) with the participation of ultrasounds at $z = 0.127$ m (1/2λ), and (c) with the participation of ultrasounds at $z = 0.1905$ m (3/4λ), visible scale-1 mm/div

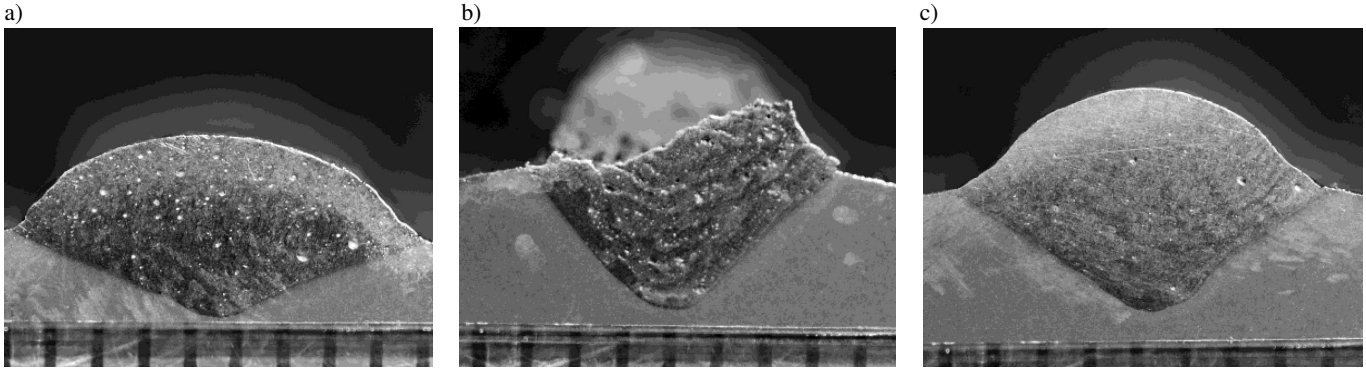

Fig. 11. Cross-section of the MIG welds: (a) without ultrasounds, (b) with the participation of ultrasounds at $z = 0.127$ m (1/2λ), and (c) with the participation of ultrasounds at $z = 0.1905$ m (3/4λ), visible scale-1 mm/div

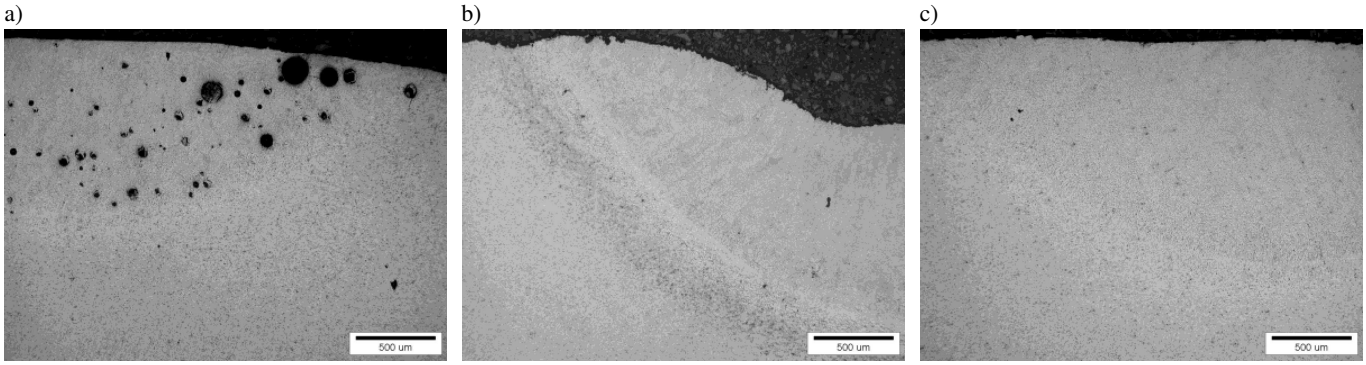

Fig. 12. Micrograph of the TIG AC welds: (a) without ultrasounds, (b) with the participation of ultrasounds $z = 0.127$ m (1/2λ), and (c) with the participation of ultrasounds $z = 0.1905$ m (3/4λ)

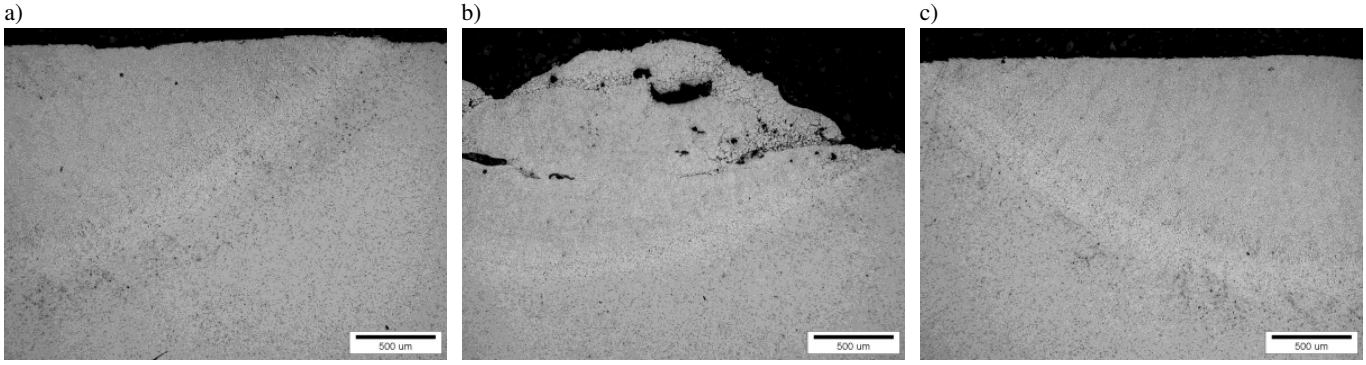

Fig. 13. Micrograph of the TIG DC welds: (a) without ultrasounds, (b) with the participation of ultrasounds z=0.127m (1/2λ), and (c) with the participation of ultrasounds z=0.1905m (3/4λ)

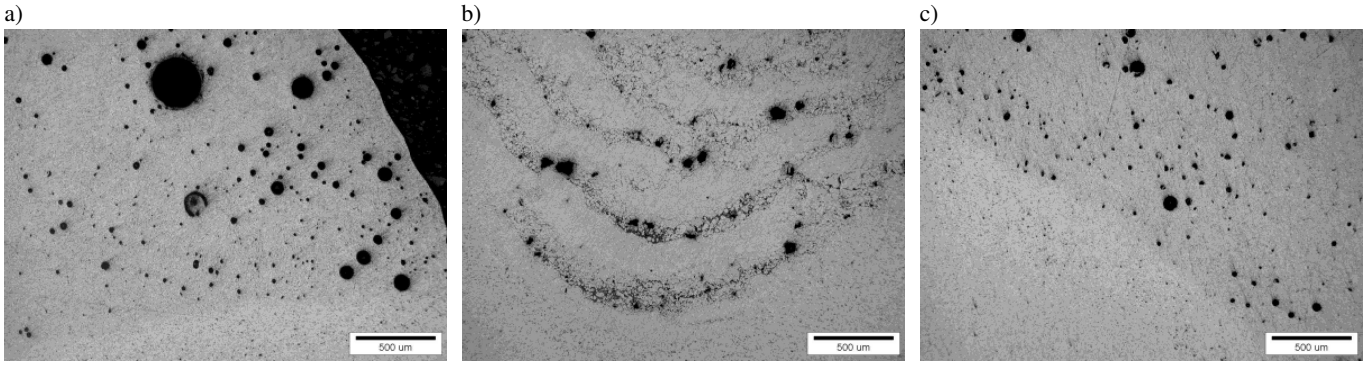

Fig. 14. Micrograph of the MIG welds: (a) without ultrasounds, (b) with the participation of ultrasounds $z = 0.127$ m ($1/2\lambda$), and (c) with the participation of ultrasounds $z = 0.1905$ m ($3/4\lambda$)

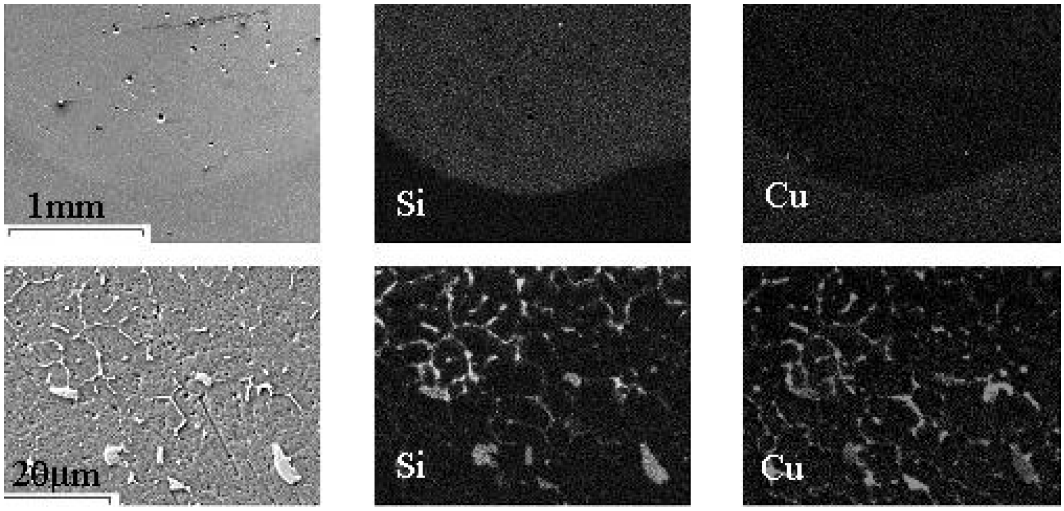

Fig. 15. Si and Cu concentrations in the cross-section weld produced by the MIG method without the ultrasounds

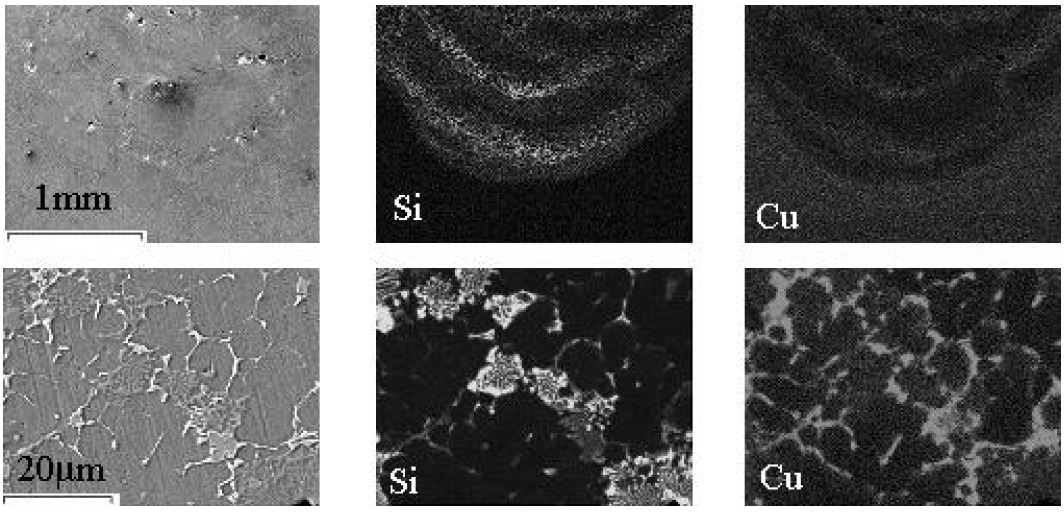

Fig. 16. Si and Cu concentrations in the MIG the cross-section weld obtained with the ultrasound assistance, $z = 0.127$ m

In MIG welding the subsequent stages of solidification of the molten pool are well visible (Fig. 14b) – they are represented by the lighter-color lines arranged circumferentially at every few μm beginning from the fusion line up to the weld face boundary. The microscopic observations have shown that the welds have a band-structure, especially after the MIG processes. We decided to examine their cross-sections welds morphology by SEM+EDX JSM-7600F, JEOL Co (Figs. 15–21).

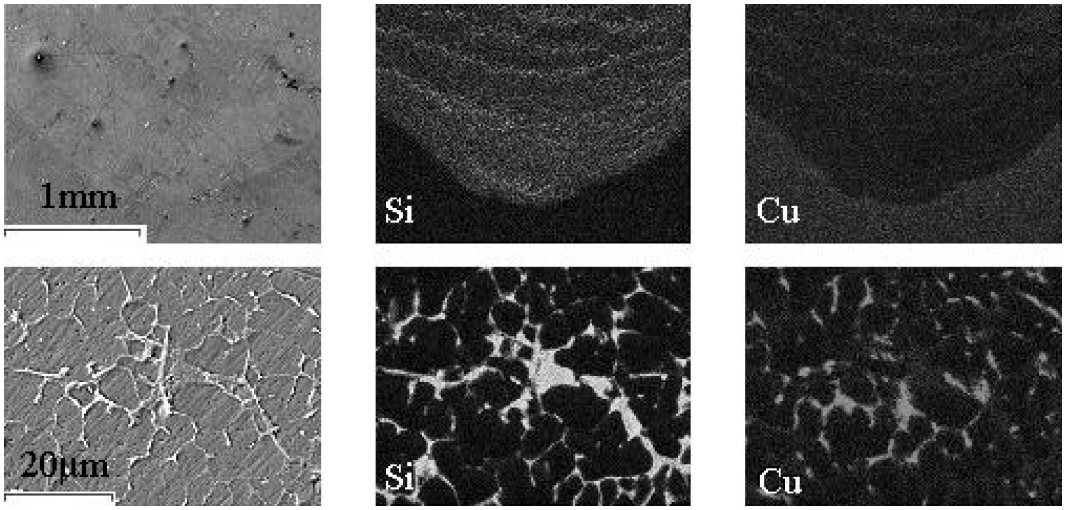

Fig. 17. Si and Cu concentrations in the MIG the cross-section weld obtained with the ultrasound assistance, $z = 0.1905$ m

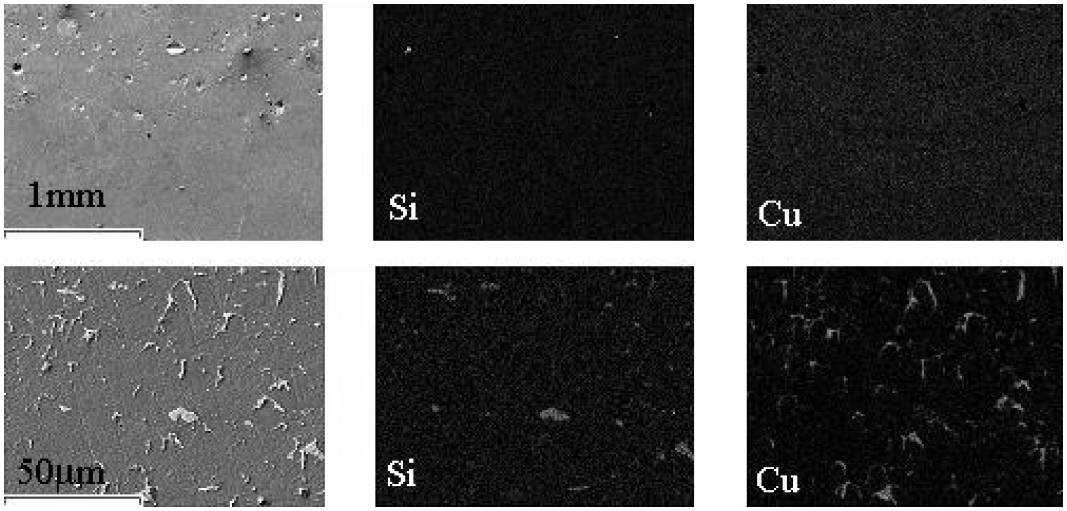

Fig. 18. Si and Cu concentrations in the cross-section weld produced by the TIG AC without the ultrasounds

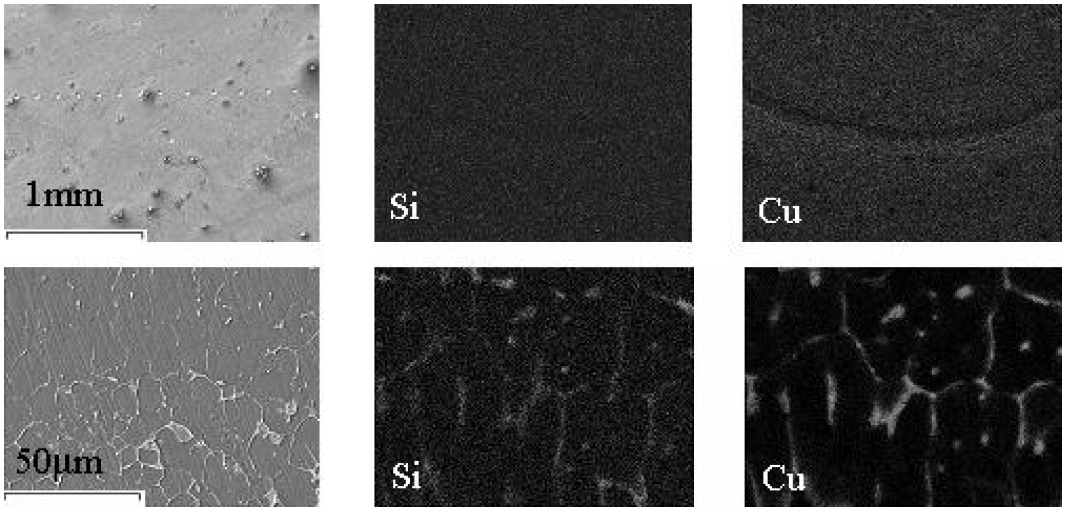

Fig. 19. Si and Cu concentrations in the TIG AC the cross-section weld obtained with the ultrasound assistance, $z = 0.1905$ m

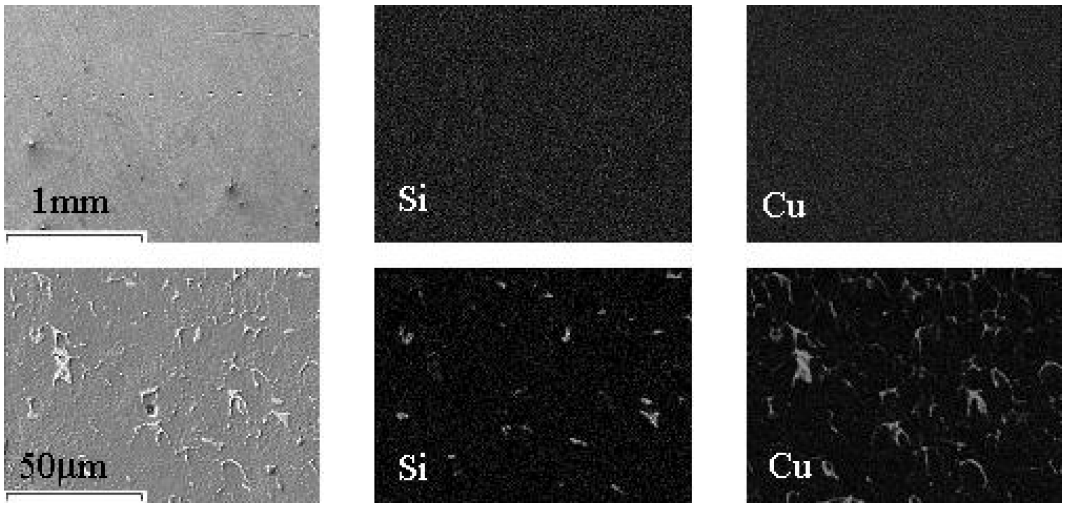

Fig. 20. Si and Cu concentrations in the cross-section weld produced by the TIG DC without the ultrasounds

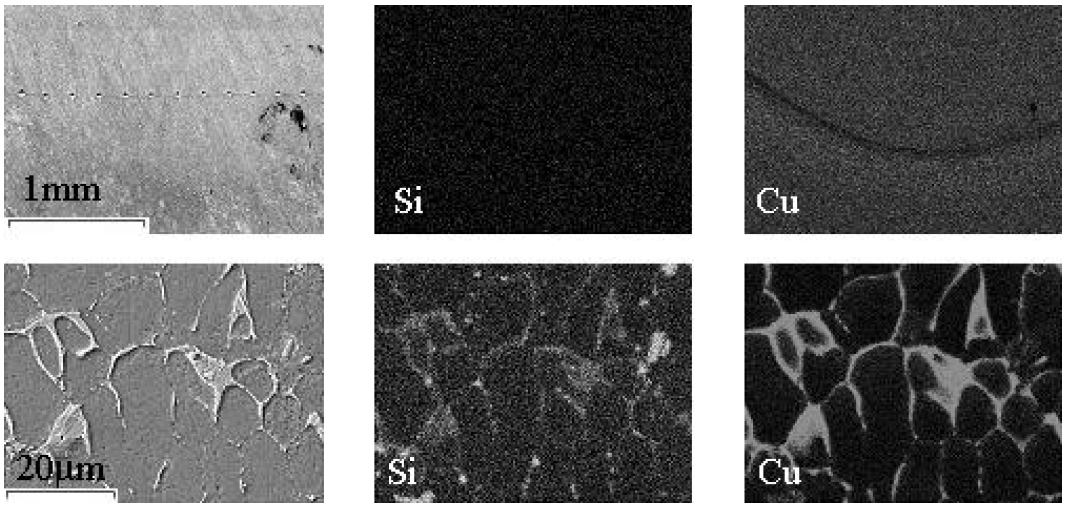

Fig. 21. Si and Cu concentrations in the TIG DC the cross-section weld obtained with the ultrasound assistance, $z = 0.1905$ m

It can be seen that within the bands the concentrations of silicon and copper are increased, especially in MIG welds obtained with the participation of ultrasounds at $z = 0.127$ m (Fig. 16). The band structure also occurs at $z = 0.1905$ m but here it is not so marked (Fig. 17). At the nodes of the vibration wave the structure appeared to be more advantageous than at its maximum displacement. The structures obtained after the TIG AC/DC welding behave in the same manner. In Figs. 18–21 we can see that Si and Cu have precipitated from the solid solution. This effect occurs in both AC- and DC-welded samples, but in DC welding it is especially intensive. As already mentioned, the DC welding is not used for aluminum alloys because of the difficulties with the removal of aluminum oxide, but when the welding process is conducted with the participation of mechanical vibrations, it is possible to obtain an acceptable structure free of the characteristic porosity (Fig. 10c). As can be seen in the photographs of the welds, the phase of the ultrasonic wave has an essential effect on the appearance of the face of the weld, on its width, and on the height of the excess weld metal. Referring to the theoretical shape of an ultrasonic wave shown in Figs. 1 and 2, we can see that the critical changes occur in the vicinity of its nodes and near its maximum displacement.

We can also notice that the weld has become scorched in the maximum displacement regions (at the mid-length of the waveguide - z=0.127m) in both the TIG, and MIG welds. These scorches are evidence that the gaseous protection was insufficient. It can therefore be supposed that, in these regions, the ultrasonic vibrations induce an effect similar to the lateral suction of air, so that the argon blown from the torch gas nozzle (11 l/min in TIG and 17 l/min in MIG) appears insufficient to ensure the effective protection. It is probable that this effect is due to the 'air cushion' formed as a result of the acoustic pressure of the vibrations. This is of course an undesired process and it is enhanced at the maxima of the vibration wave where in addition we have discontinuities of the weld face due to metallurgical de-cohesion of the material. It has also appeared that the shape and the proportion of the dimensions of the MIG and TIG welds vary depending on the co-ordinate z. Fig. 22 show these relationships.

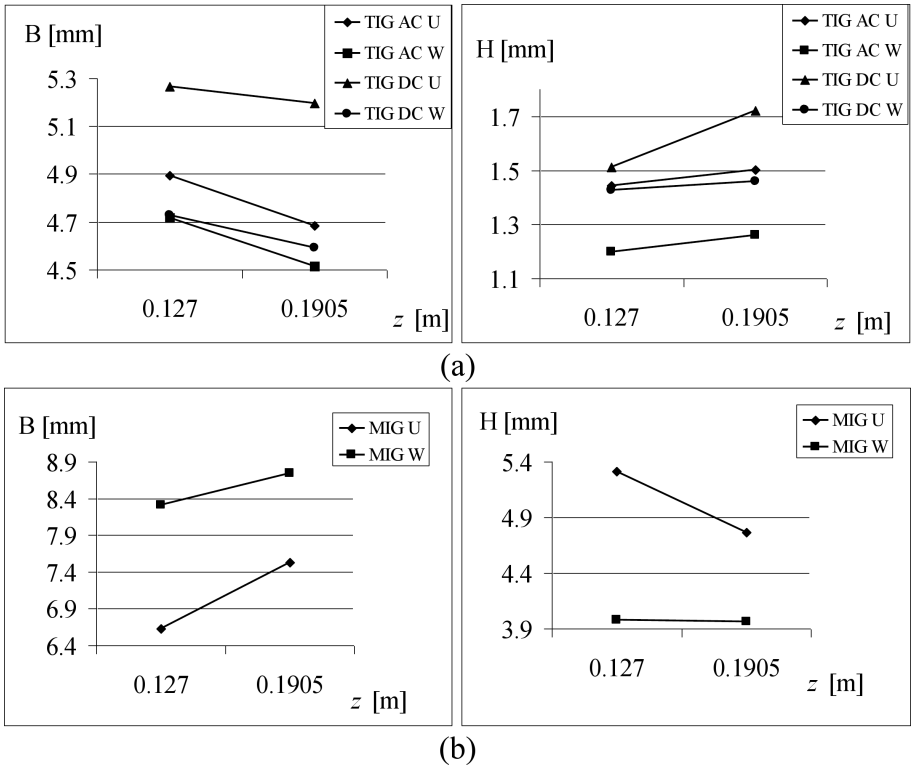

Fig. 22. Width of weld face B and penetration depth H for TIG (a) and (b) MIG welds: B – weld face with, H – depth of root penetration, U – with ultrasounds, W – without ultrasounds

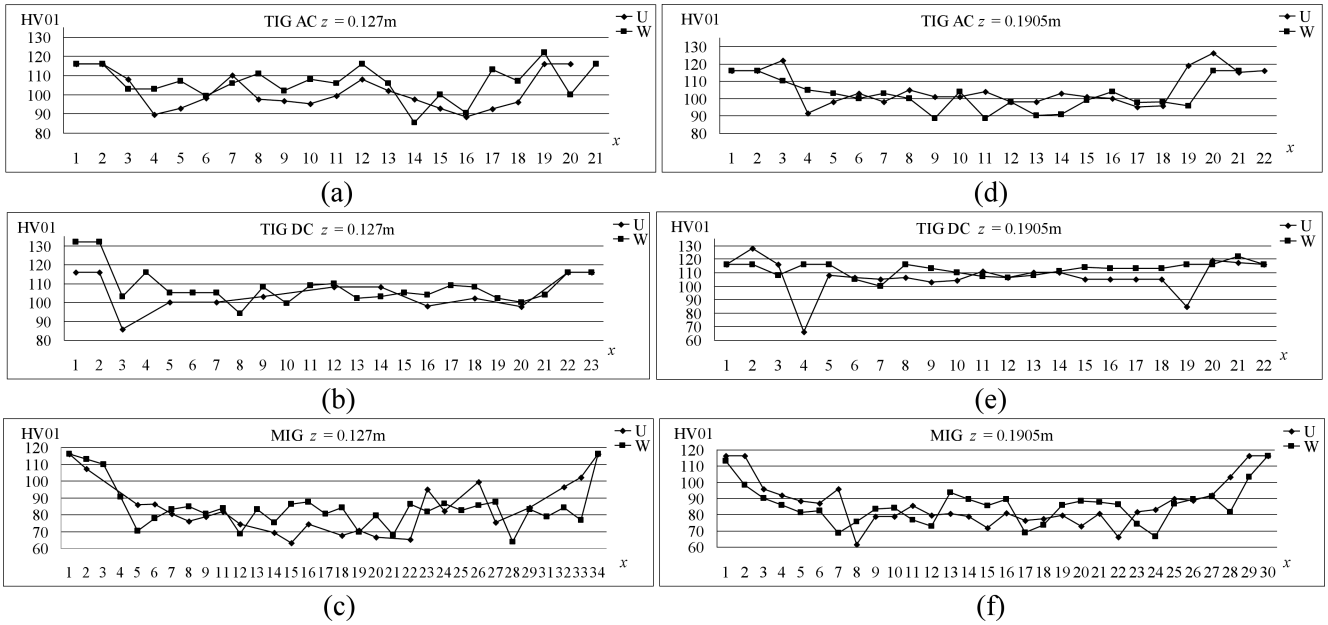

Fig. 23. Hardness distributions on transverse cross-sections of the welds produced by (U - with the assistance of ultrasounds, W-without ultrasounds, div-divisions on the x axis: (a) U – 150 μm/div, W-210 μm/div, (b) U – 210 μm/div, W – 180 μm/div, (c) U – 180 μm/div, W – 210 Mm/div, (d) U – 210 μm/div, W – 210 μm/div, (e) U – 230 μm/div, W – 240 μm/div, and (f) U – 250 μm/div, W – 250 μm/div

Hardness was measured by the Vickers method under a load of 100 g. The hardness distributions on the characteristic cross-sections of the welds are shown in Fig. 23. Each point on the diagrams is the average calculated from 4 measurements. We can see from this figure that the ultrasounds increase the uniformity of the hardness distribution, irrespective of the measurement co-ordinate z, but in general, they decrease the hardness values, regardless of the welding method employed and the co-ordinate z. An exception is the case of the TIG AC weld shown in Fig. 23d,e which, when compared

with the TIG DC weld shown in Fig. 23e, shows something quite opposite. There are two places in HAZ were the microhardness instantly dropping down.

4. Discussion

To interpret properly the structure of the characteristic regions of the welds obtained by the TIG and MIG methods we analyzed the conditions that prevailed during the thermal cycles to which the materials were subjected. The temperature distribution of the interest region laying at distance z from heat source was calculated using conventional formula for the semi infinity body, quasi-stationary temperature distribution, considering the concentrated heat source [27–30].

The changes of the temperature were evaluated in dependence on the welding process parameters adopted in the experiments, the thermal properties of the 2017 alloy, and the co-ordinate z. Figure 24 shows the results of the analysis, from which it follows that the distance between the crystallization fronts, at a depth of $y = 0.001$ m (1 mm) beneath the outside surface (the depth at which metallographic cross-sections are usually prepared) is 0.0033 m (3.3 mm) in the TIG welding, and above 0.001 m (1 mm) in MIG.

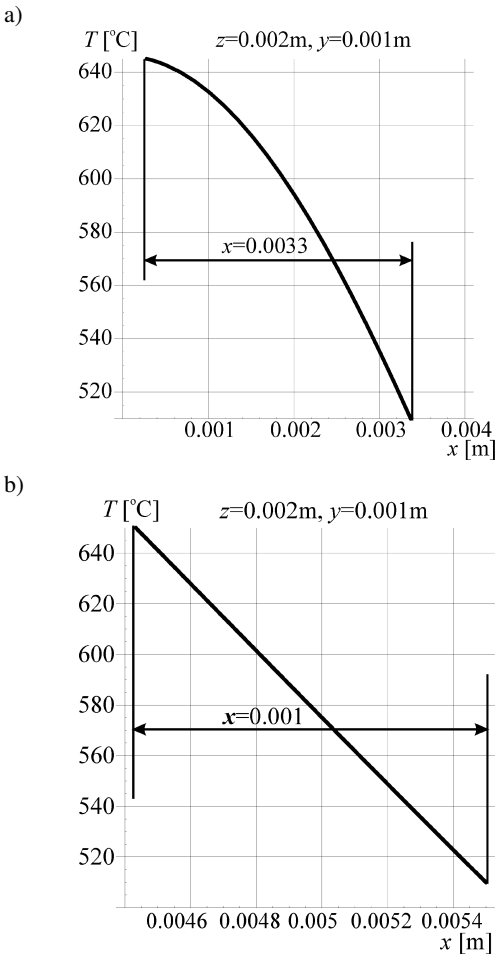

Fig. 24. Distribution of the temperature in TIG (a) and MIG welding (b)

The results presented above do not take into account the heat exchange with the environment or radiation and, thus, they are estimates of the upper limit of the possible values. Nevertheless we can try to draw some conclusions by confronting the structures shown in Figs. 12b and 13b with the results of the analysis. We can clearly see from this confrontation that, especially in ultrasound-enhanced MIG welding, the distance between the successive crystallization fronts can be estimated at 0.0005 m (0.5 mm) which is half the distance inferred from Fig. 24b. It is of course not obvious at this stage of our experiments that this distance decreased thanks to the participation of ultrasounds, but this seems possible.

In the case of TIG welding, the diagram of Fig. 24a suggests that this distance is about 0.0033 m, a value comparable with the depth of the fusion-weld (Figs. 12b and 13b). The results of the thermal analysis cannot reliably be compared with the TIG structure, since, probably, the amount of the liquid phase in the molten pool is here not large enough to let the phenomena that permit manifesting the crystallization fronts to take place.

It is also worth noting that, during free solidification of the weld obtained without the participation of ultrasounds, no sequence of the crystallization fronts is observed (Figs. 12a, 13a). It is probable that the high-power ultrasonic vibrations alter the dynamics of free solidification during which the crystallization fronts are mechanically disintegrated. Another reason may be that, as a result of the vibrations, all the alloying constituents and impurities tend to settle on the boundaries of the successive crystallization fronts.

Our experiments have shown that the advantageous effects can only be achieved when the ultrasonic vibrations are in the 3/4λ phase ($z = 0.1905$ m) i.e., at the vibration nodes. At the distances corresponding to the vibration maximum displacement (1/2λ, $z = 0.127$ m), the weld-face is de-cohered to the disqualifying degree, and its structure becomes markedly band-shaped with clearly visible crystallization fronts. The saw-toothed discontinuities of the weld-face (Figs. 6b, 7b, and 8b) are probably due to the substitutive stresses σ_Z whose magnitude is about 10–13 MPa (Fig. 2). At an elevated temperature this results in the cohesion of the weld-face material being exceeded.

5. Conclusions

- In ultrasound-assisted welding, the weld quality can only be improved if the substitutive stresses σ_R are compressive, at the faze 3/4λ nodes. If this is so, we achieve an advantageous refining of the material, the porosity is reduced, and no mechanical de-cohesion of the weld-face occurs. Moreover the hardness of the heat affected zone (HAZ) decreases. In TIG welding the face of the weld is narrower but its penetration depth increases, whereas in MIG welding the converse holds true.
- At the maximum displacement of the vibrations, i.e., at faze 1/2λ and λ, the weld-face undergoes mechanical de-cohesion, the gaseous protection becomes ineffective, and the solidified material has a band-structure. Another effect

observed during the ultrasound-assisted arc MIG and TIG welding of the 2017A alloy is the precipitation of silicon and copper from the solid solution, chiefly at the maximum displacement of the vibration wave (faze $3/4\lambda$). In TIG welding, the face width and weld penetration depth increase, whereas after MIG welding the face is narrower. No good shielding gas protection can be achieved during welding process.

REFERENCES

[1] A. Krajewski, "Welding processes supported by mechanical vibration", *Science Bulletin. Mechanics Series*, *Innovations in Joining Techniques* 229, 33–51 (2009).

[2] A. Krajewski, "The investigation of the effect of ultrasound field on the weld structure and properties", *Science Bulletin. Mechanics Series* 230, 71–82 (2010).

[3] A. Krajewski, "Mechanical vibrations in the welding processes", *Welding Technology Review* 6, 37–42 (2011).

[4] H. Longbiao, W. Minsheng, L. Luming, and H. Hongwei, "Ultrasonic generation by exciting electric arc: A tool for grain refinement in welding process", *Applied Physics Letters* 89, 131–504 (2006).

[5] L. Yu-Cheng, W. Zhi-Wei, and C. Xi-Zhang, "Effect of arc ultrasound on microstructures and mechanical properties of plasma arc welded joints of SiCp/Al MMCs", *Trans. Nonferrous Metals Society of China* 21, 272–277 (2011).

[6] M. Farrow, *Laser/Ultrasonic Welding Technique*, United States Patent 4330699 (1982).

[7] D. Weng-Long, "Effects of high-intensity ultrasonic-wave emission on the weldability of aluminum alloy 7076-T6", *Materials Letters* 57, 2447–2454 (2003).

[8] H. Dong, L. Yang, C. Dong, and S. Kou, "Improving arc joining of Al to steel and Al to stainless steel", *Materials Science and Engineering* A 534, 424–435 (2012).

[9] K. Balasubramanian, "Studies on the effect of vibration on hot cracking and grain size in AA7075 aluminum alloy welding", *Int. J. Engineering Science and Technology* 3, 1 (2011).

[10] L. Qingmei, Z. Yong, S. Yoling, Q. Feipeng, and Z. Qijie, "Influence of ultrasonic vibration on mechanical properties and microstructure of 1Cr18N9Ti stainless steel", *Materials and Design* 28, 1949–1952 (2007).

[11] Y. Cui, C. Xu, Q. Han, "Effect of ultrasonic vibration on unmixed zone formation", *Scripta Mater.* 55, 975–978 (2006).

[12] D. Weng-Long, *Effects of high-intensity ultrasonic-wave emission on the weldability of aluminum alloy 7076-T6*, Materials Letters 57, 2447–2454 (2003).

[13] S. Kim., T. Watanabe, and Y. Yoshida, "Ultrasonic vibration aided laser welding of Al alloys: improvement of laser welding-quality", *J. Laser Aplications* 7 (1), 38–46 (1995).

[14] W. Weite, "Influence of vibration frequency on solidification of weldments", *Scripta Mater.* 42, 661–665 (2000).

[15] X. Zhiwu, Y. Jiuchun, W. Gaohui, K. Xiangli, and Y. Shipin, "Interface structure of ultrasonic vibration aided interaction between Zn–Al alloy and Al_2O_3p/6061Al composite", *Composites Science & Technology* 65, CD-ROM (2005).

[16] T. Chmielewski and D. Golański, "New method of in-situ fabrication of protective coatings based on Fe-Al intermetallic compounds", *Proc. Mechanical Engineers Part B-J. Engineering Manufacture* B4 225, 611–616 (2011).

[17] J. Piekoszewski, A. Krajewski, F. Prokert, J. Senkara, J. Stanisławski, L. Waliś, Z. Werner, and W. Włosiński, "Brazing of alumina ceramics modified by pulsed plasma beams combined with arc PVD treatment", *Vacuum* 70 (2–3), 307–312 (2003).

[18] W. Włosiński, A. Krajewski, J. Piekoszewski, J. Stanisławski, and L. Waliś, "Intense pulsed plasma beams in ceramic/metal brazing", *Nukleonika* 45 (2), 145–1463 (2000).

[19] W. Włosiński and T. Chmielewski, "Plasma-hardfaced chromium protective coatings-effect of ceramic reinforcement on their wettability by glass", *Contributions of Surface Engineering to Modern Manufacturing and Remanufacturing* 1, 48–53 (2002).

[20] M. Chmielewski and K. Pietrzak, "Processing, microstructure and mechanical properties of Al_2O_3-Cr nanocomposites", *J. Eur. Ceramic Society* 27 (2–3) 1273–1279 (2007).

[21] J. Braszczyński, "The mechanism of the influence of vibration on the crystallization of cast alloys", *Mem. Etud. Sci. Rev. Metall.* 80 (1), 27–36 (1983).

[22] L. Mingyu, J. Hongjun, W. Chunqing, B. Han Sur, and B. Hee Seon, "Interdiffusion of Al-Ni systems enhanced by ultrasonic vibration at ambient temperature", *Ultrasonics* 45, 61–65 (2006).

[23] A. Krajewski, "Joining of Si_3N_4 to wear-resistant steel by direct diffusion bonding", *J. Materials Processing Technology* 54 (1–4), 103–108 (1995).

[24] W. Węglewski, M. Basista, M. Chmielewski, and K. Pietrzak, "Modeling of thermally induced damage in the processing of Cr-Al_2O_3", *Composites Part B-Engineering* 43 (2), 255–264 (2012).

[25] R. Kumar, M. Panchal, "Study of circular crested waves in a micropolar porous medium possessing cubic symmetry", *Bull. Pol. Ac.: Tech.* 59 (1), 103–110 (2011).

[26] R. Kumar, A. Miglani, and S. Kumar, "Reflection and transmission of plane waves between two different fluid saturated porous half spaces", *Bull. Pol. Ac.: Tech.* 59 (2), 227–234 (2011).

[27] L. Chon and M. Chin, *Heat Flow in Fusion Welding*, in *Welding, ASM Hand Book, Brazing, and Soldering*, vol. 6, ASM The Materials Information Society, London, 1993.

[28] L. Olejnik, A. Rosochowski, "Methods of fabricating metals for nano-technology", *Bull. Pol. Ac.: Tech.* 53 (4), 413–423 (2005).

[29] E. Kannatey-Asibu jr, W. Włosiński, and A. Krajewski, "New methods of solid-state joining thin-wall elements made of aluminum alloys", *Archives of Metallurgy and Materials* 53 (3), 669–678 (2008).

[30] Z. Lindeman, K. Skalski, W. Włosiński, J. Zimmerman, "Thermo-mechanical phenomena in the process of friction welding of corundum ceramics and aluminium", *Bull. Pol. Ac.: Tech.* 54 (1), 1–8 (2006).